Functional Materials 13, No.3 (2006)

Chemical synthesis of nanocrystalline Ni–Zn ferrites and their magnetic characteristics

Jong-Chul Lee[*], *D.Caruntu*[**], *Joon-Hyung Lee*[*], *Jeong-Joo Kim*[*], *B.Cushing*[**], *V.Golub*[**], *Sang-Hee Cho*[*,**], *C.J.O'Connor*[**]

[*]Department of Inorganic Materials Engineering,
Kyungpook National University, Daegu, 702-701, Korea
[**]Advanced Materials Research Institute (AMRI)
University of New Orleans, New Orleans, LA 70148, USA

Nanocrystalline $Ni_{1-x}Zn_xFe_2O_4$ powders were synthesized by the citrate precursor method, and the reaction sequence during the process was examined. Studies of the reaction sequence showed that a $NiFe_2O_4$ phase was developed as soon as the metal citric acids were thermally decomposed. In the case of $ZnFe_2O_4$, however, ZnO and Fe_2O_3 were produced first when the metal citric acids were decomposed at low temperature. A single phase of $ZnFe_2O_4$ was subsequently obtained when a heat treatment was conducted at 500°C for 2 h. On the other hand, in order to examine the effect of particle size on magnetic characteristics of Ni–Zn ferrites, nanocrystalline $Ni_{1-x}Zn_xFe_2O_4$ powders with particle sizes of approximately 7, 25 and 100 nm were prepared by coprecipitation and citrate precursor methods. The magnetic characteristics of the ultrafine (7 nm) and coarse (100 nm) nanocrystalline ferrites showed distinct differences. These differences are attributed to cation disordering at the surfaces of particles, which becomes increasingly dominant as the particle size decreases.

Методом цитратов-прекурсоров синтезированы нанокристаллические порошки $Ni_{1-x}Zn_xFe_2O_4$ и рассмотрена последовательность реакций в этом процессе. Изучение последовательности реакций показало, что непосредственно после термического разложения цитратов металлов образовалась фаза $NiFe_2O_4$. Однако в случае $ZnFe_2O_4$ при разложении цитратов металлов при низкой температуре вначале образовывались ZnO и Fe_2O_3. Затем в процессе термообработки при 500°C в течение 2 ч получена одна фаза $ZnFe_2O_4$. С другой стороны, с целью исследования влияния размера частиц на характеристики Ni–Zn ферритов нанокристаллические порошки $Ni_{1-x}Zn_xFe_2O_4$ с размерами частиц приблизительно 7, 25 и 100 нм получены соосаждением и методом цитратов-прекурсоров. Выявлены существенные различия в магнитных характеристиках ультратонких (7 нм) и крупнозернистых (100 нм) нанокристаллических ферритов. Эти различия приписаны катионному разупорядочению на поверхностях частиц, преобладание которого возрастает при уменьшении размеров частиц.

Ferrimagnetic oxides, known as ferrites, can be expressed as $M^{2+}O{\cdot}Fe_2^{3+}O_3$ in which M^{2+} is a divalent metal ion such as Mg^{2+}, Ni^{2+}, Fe^{2+} or Cu^{2+}. A wide range of ferrite compositions with different magnetic properties can be prepared by varying and/or mixing M^{2+} cations. The magnetic properties of the spinel-structured Ni–Zn ferrites ($Ni_{1-x}Zn_xFe_2O_4$) exhibit the strongest composition dependence among the known ferrite materials. The magnetic characteristics of bulk Ni–Zn ferrite prepared by solid state reaction have been reported [1]. The mixed ferrite $Ni_{1-x}Zn_xFe_2O_4$, where Ni is a divalent ion, is a solid solution in which the magnetic moment varies as a function of Zn content. The incorporation of up to about 50 % Zn increases the magnetization, which then decreases toward zero for pure Zn ferrite [2].

Recently, scientific interest has been increasingly focused on the synthesis and characterization of nano-structured solids.

The characteristics of nanocrystalline powders greatly depend on surface effects that become increasingly dominant as particle size decreases and surface area increases. Therefore, as micron-sized powders are brought into the nano-size regime, new characteristics are expected to appear that cannot be expected in bulk or micron powders [3], such as the paramagnetization of ferromagnetics, changes of band gap and the formation of metastable phases [4]. These results suggest that systematic investigations of the novel properties of nano powders are warranted.

Nanocrystalline ferrite powders have been prepared by various methods, including coprecipitation [5,6], sol-gel [7,8], hydrothermal [9,10] and citrate precursor methods [11]. The reaction sequence of bulk Ni–Zn ferrite in solid state reaction and molten salt reaction has been reported [12, 13]. It was found that $ZnFe_2O_4$ formed first by the reaction between Fe_2O_3 and ZnO at low temperature, then Ni–Zn ferrite formed by the reaction between NiO and $ZnFe_2O_4$ at higher temperature.

In this study, nanocrystalline Ni–Zn ferrite powders were manufactured using one of the simplest manufacturing methods of the citrate precursor method. From the experimental results, a reaction sequence for the nanocrystalline ferrites is suggested. On the other hand, nanocrystalline Ni–Zn ferrite powders with particle sizes around 7, 25 and 100 nm were manufactured using the coprecipitation and citrate precursor methods, respectively, in order to examine the effects of particle size on magnetic characteristics.

Nanocrystalline $Ni_{1-x}Zn_xFe_2O_4$ ($0 \le x \le 1$) was prepared by the citrate precursor method. High purity raw chemicals of citric acid ($C_6H_8O_7$), nickel nitrate ($Ni(NO_3)_2 \cdot 6H_2O$), zinc nitrate ($Zn(NO_3)_2 \cdot 6H_2O$) and ferric citrate ($FeC_6H_5O_7$) were used. The ferric citrate and the citric acid were weighed with 1:1 mole fraction and dissolved together with distilled water at 60°C for 40 min in a bath. The nickel nitrate and the zinc nitrate corresponding to the target compositions were weighed and dissolved slowly in a continuously stirred bath of the ferric citrate and the citric acid solution. The precursor mixtures were then continuously heated at 60°C with constant stirring to obtain dried products that were in the form of a uniformly colored, brown transparent glass containing all the cations homogeneously mixed at the atomic level. The mixtures were dried at 100°C for 72 h. The dried citrate precursors were heat-treated in a furnace at 250–500°C for 2 h with a heating rate of 5°C/min. DTA-TG (Mettler Toledo TGA/SDTA 851^e, Switzerland) analysis was conducted in the temperature range 25–700°C with a heating rate of 5°C/min in air for the identification of weight losses and decomposition temperatures.

In order to obtain finer nano powders, another processing method involving a coprecipitation route was employed. Raw materials of $NiCl_2 \cdot 6H_2O$ (99.9999 %), $ZnCl_2$ (99.99 %) and $FeCl_3$ (99.99 %) were used as starting chemicals for coprecipitation of $Ni_{1-x}Zn_xFe_2O_4$ ($0.0 \le x \le 1.0$). The starting chemicals were dissolved separately in distilled water and subsequently mixed. The mixed solution was kept below pH = 1 to avoid precipitation. The Ni–Zn ferrite solution was added dropwise to a continuously stirred bath of aqueous NH_4OH with a pH adjusted to 10. After ageing, the precipitates were filtered, washed to remove chloride ions and then dried at 120°C for 24 h. The dried products were calcined in a furnace at 300° for 1 h with a heating rate of 3°C/min.

Elemental analysis of the calcined powders prepared by the citric precursor and the coprecipitation methods was carried out by ICP. For samples of identical nominal composition, no considerable compositional differences in the powders prepared by the different methods were observed. Powder X-ray diffraction with nickel-filtered Cu–K_α radiation (MO3-XHF, MAC Science Co., Japan) was used for phase identification. The Vibrating Sample Magnetometer (VSM: LDJ 9600, USA) at 15,000 Oe and 300 K was used for the characterization of magnetic properties of the powders. In addition, morphological characteristics of the nanocrystalline ferrite powders were investigated by transmission electron microscopy.

Reaction sequence of Ni–Zn ferrite in the citrate precursor method. Fig. 1 shows the DTA-TG analysis of the chelated metal citric acids of the starting chemicals — nickel citric acid, zinc citric acid and iron citric acid. In the case of nickel citric acid, a sharp and monotonous exothermal peak appeared when a drastic weight loss occurred around 350°C. In the case of iron citric acid, a drastic weight loss appeared around 200°C and a corresponding sharp exothermal peak was observed. Complex mass losses and thermal events were observed in the case of zinc citric acid and the decompo-

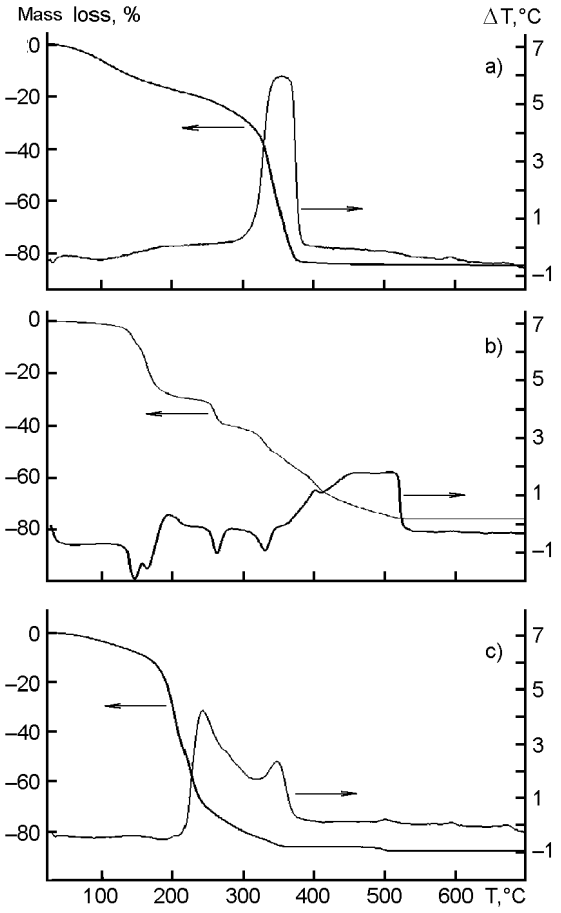

Fig. 1. DTA-TG curves of the chelated metal cirtic acids of the starting chemicals; (a) nickel citric acid, (b) zinc citric acid and (c) iron citric acid.

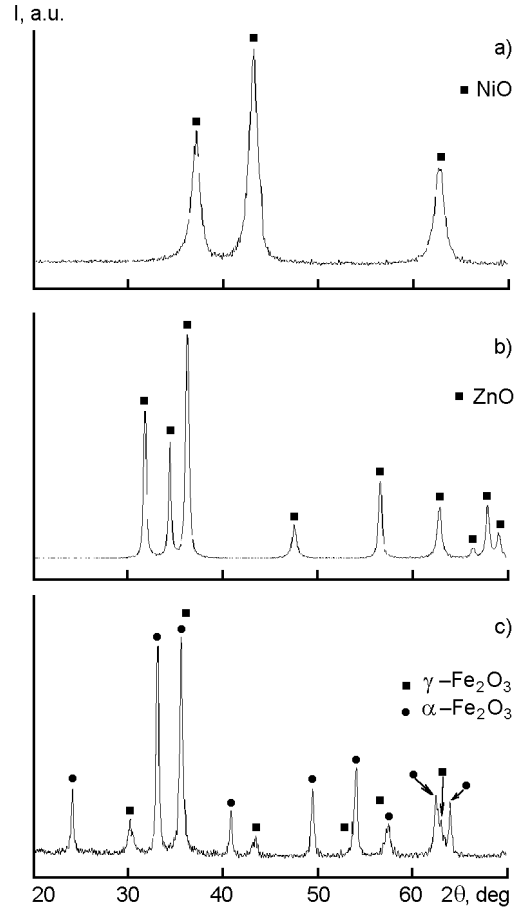

Fig. 2. X-ray diffraction patterns of (a) the nickel, (b) zinc and (c) iron citric acids after a heat treatment at 375, 525, 360°C, respectively.

sition temperature was extended up to 525°C. From this result, we can recognize that the decomposition temperatures of the various metal citric acids differ the zinc complex exhibited the highest decomposition temperature. The starting chemicals of the metal citric acids likely decompose into oxides at 375, 525 and 360°C for the nickel, zinc and iron citric acid complexes, respectively, where the mass %. plateaus.

Fig. 2 shows the X-ray diffraction patterns of the metal citric acids after a heat treatment at the decomposition temperature where the weight losses end. The metal citric acids of the nickel, zinc and iron were heat treated in air to their respective decomposition temperatures of 375, 525 and 360°C with a heating ramp of 5°C/min. As soon as the temperature reached the respective target temperature, the metal citric acids were air quenched. As shown in the Fig. 2, the metal citric acids decompose into oxides after the heat treatment at the decomposition temperature. In the case of the iron citric acid, however, two kinds of iron oxides — γ–Fe_2O_3 [14] and α–Fe_2O_3 [15]) — coexisted. At higher temperatures, the metastable γ–Fe_2O_3 phase transforms to α–Fe_2O_3 [16].

Fig. 3 shows the TEM photographs of the NiO, ZnO and Fe_2O_3 after decomposition from metal citric acids at their decomposition temperature of 375, 525 and 360°C. The particle size of the NiO, ZnO and Fe_2O_3 was about 6, 70 and 25 nm, respectively. Severe agglomeration was observed in ZnO.

Fig. 4 shows the DTA-TG analysis of the mixtures of metal citric acids corresponding to the compositions of $NiFe_2O_4$, $ZnFe_2O_4$ and $Ni_{0.5}Zn_{0.5}Fe_2O_4$. $NiFe_2O_4$ precursor shown in Fig. 3(a) revealed two clear exothermal peaks around 240 and 320°C, which originated from iron and nickel citric acid, respectively. When zinc citric acid was incorporated into $Ni_{0.5}Zn_{0.5}Fe_2O_4$ and

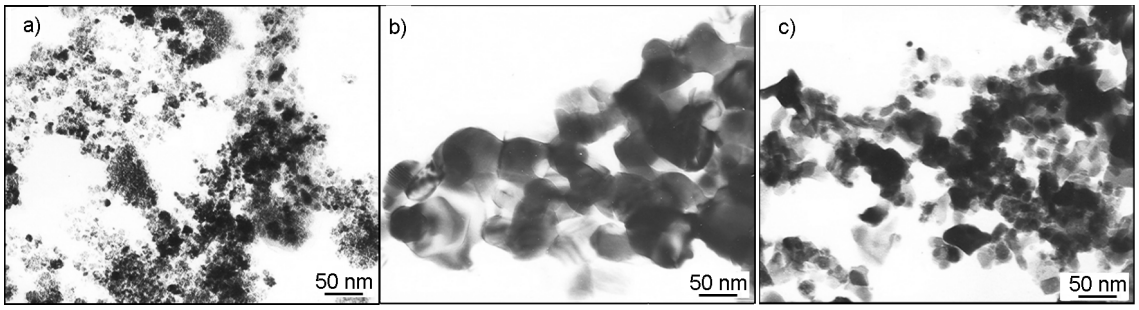

Fig. 3. TEM photographs of the (a) NiO, (b) ZnO and (c) Fe_2O_3 after decomposition from metal citric acids at their decomposition temperature of 375, 525 and 360°C.

$ZnFe_2O_4$ precursors, smooth and complex exothermal peaks appeared, probably resulting from the complex thermal events of the decomposition of zinc citric acid as shown in Fig. 1(b). The mass loss observed below 100°C is due to the volatilization of H_2O adsorbed on the surface of the citrate precursor. The additional mass loss of approximately 35 mass % observed between 100 and 200°C likely results from the volatilization of coordinated H_2O molecules of the citrate precursors. The mass loss that occurs over 200°C is attributed to the decomposition of organic material in the citrate precursors. The temperature of a complete burn-off of organic substances without any further weight loss for $NiFe_2O_4$, $Ni_{0.5}Zn_{0.5}Fe_2O_4$ and $ZnFe_2O_4$ was about 340, 370 and 410°C, respectively, showing a tendency for an increase in the decomposition temperature with increasing zinc citric acid content. The decomposition temperatures of the mixed-metal citric acids ($NiFe_2O_4$, $Ni_{0.5}Zn_{0.5}Fe_2O_4$ and $ZnFe_2O_4$ precursors) decreased compared to those of the single-metal citric acid complexes.

Fig. 5 shows the XRD patterns of $NiFe_2O_4$, $ZnFe_2O_4$, and $Ni_{0.5}Zn_{0.5}Fe_2O_4$ precursors heat-treated in the temperature range between 300 and 500°C without isothermal holding time and with an isothermal holding time of 2 h at 500°C. $NiFe_2O_4$ and $ZnFe_2O_4$ precursors were amorphous when the precursors were heat-treated at 300°C. Despite a more than 90 % mass loss by 300°C, crystallization has not yet substantially progressed. In the case of the $NiFe_2O_4$ precursor, the $NiFe_2O_4$ phase appears to form directly at the temperature where the nickel and iron citric acids are completely decomposed. In the case of $ZnFe_2O_4$, however, Fe_2O_3 and ZnO phases formed at 400°C. $ZnFe_2O_4$, Fe_2O_3 and ZnO phases coexisted even when the temperature was increased to 500°C and single-phase

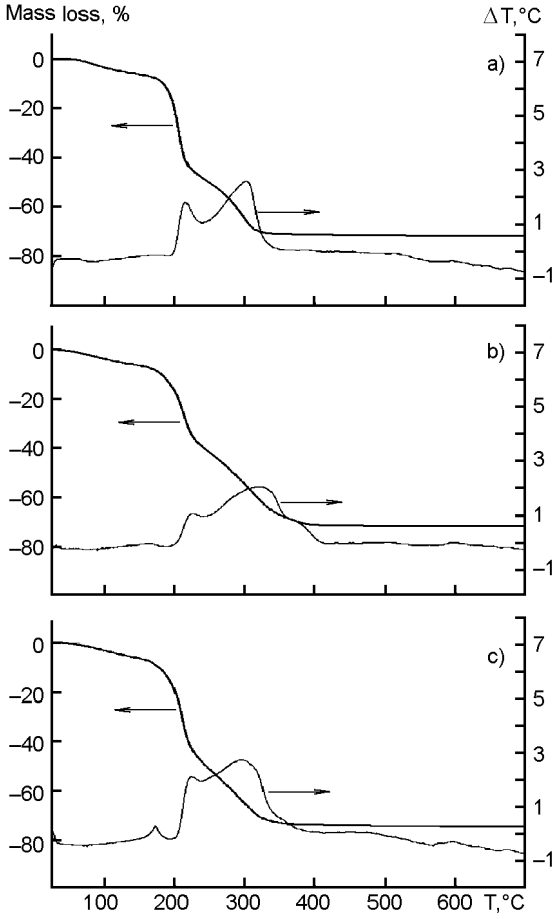

Fig. 4. DTA-TG curves of the (a) $NiFe_2O_4$, (b) $ZnFe_2O_4$ and (c) $Ni_{0.5}Zn_{0.5}Fe_2O_4$ precursors.

$ZnFe_2O_4$ was not obtained at this temperature. Because the heat treatment temperature is quite low compared to a traditional solid state reaction, long-range diffusion of ions is kinetically limited during crystallization. Consequently, intermediate or metastable inhomogeneous phases often crystallize. The larger ionic radius of Zn (0.74 Å) relative to those of Ni (0.69 Å) and Fe (0.63 Å) undoubtedly slows its diffusion kinetics. The great difference in particle

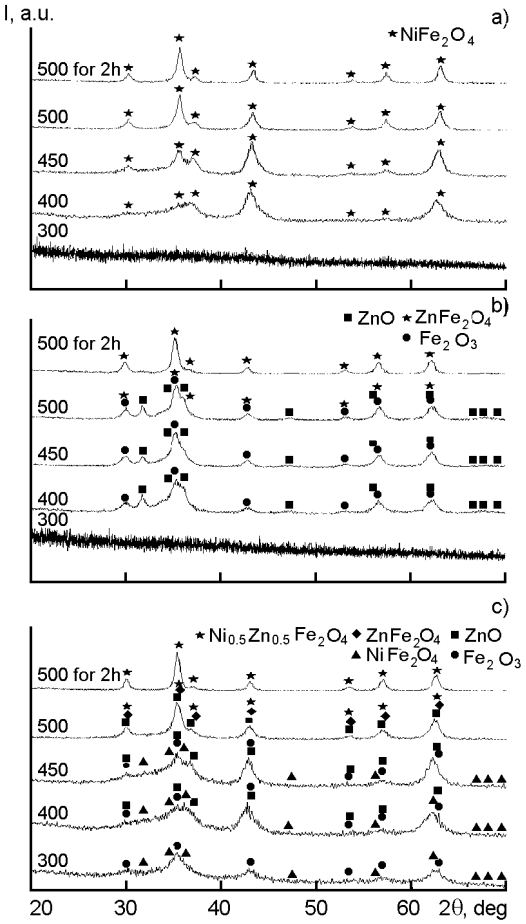

Fig. 5. X-ray diffraction patterns of (a) $NiFe_2O_4$, (b) $ZnFe_2O_4$, and (c) $Ni_{0.5}Zn_{0.5}Fe_2O_4$ precursors heat treated at 300–500°C without isothermal holding time.

size between NiO, ZnO and Fe_2O_3 after the decomposition also seems to play a partial role in the reaction. Specifically, the reaction between finely divided NiO and Fe_2O_3 takes place prior to any observable reaction involving ZnO. This observation implies that the reaction between ZnO and Fe_2O_3 to form a spinel-structured ferrite requires a higher thermal activation energy and/or longer diffusion time than the similar reaction between NiO and Fe_2O_3. Consequently, The $ZnFe_2O_4$ eventually formed a single phase after isothermal heat treatment at 500°C for 2 h, unlike $NiFe_2O_4$, which produced a single phase at 500°C without the isothermal heat treatment as shown in Fig. 5(a) and (b).

On the other hand, some degree of crystallization at 300°C was observed in $Ni_{0.5}Zn_{0.5}Fe_2O_4$, as evidenced by the broad diffraction peaks in Fig. 5(c). According to the DTA-TG analysis of $Ni_{0.5}Zn_{0.5}Fe_2O_4$, however, decomposition is not complete at

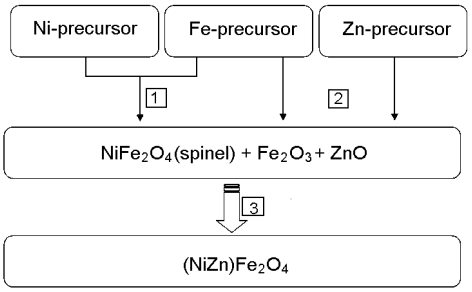

Fig. 6. Proposed mechanism of Ni–Zn ferrites formation by the citrate precursor method.

300°C. Therefore, crystallographically and thermodynamically metastable intermediate phases might be formed at this temperature. Initiation of crystallization at 300°C for $Ni_{0.5}Zn_{0.5}Fe_2O_4$ is unlikely. In the case of $Ni_{0.5}Zn_{0.5}Fe_2O_4$, a simultaneous development of $NiFe_2O_4$, Fe_2O_3 and ZnO phases probably initiates at low temperature and a single phase of $Ni_{0.5}Zn_{0.5}Fe_2O_4$ forms without isothermal heat treatment at 500°C.

A reaction sequence for the formation of nanocrystalline Ni–Zn ferritesis proposed in Fig. 6. $NiFe_2O_4$ first forms around ~400°C, followed by the reaction of ZnO and Fe_2O_3 with $ZnFe_2O_4$. Finally, the reaction between $NiFe_2O_4$, Fe_2O_3 and ZnO initiates at higher temperature. This is rationalized on the basis of the following experimental results: i) According to the DTA-TG and X-ray diffraction analysis, the formation temperature of $ZnFe_2O_4$ was higher than that of $Ni_{0.5}Zn_{0.5}Fe_2O_4$. As a result, a selective reaction between ZnO and Fe_2O_3 in the presence of $NiFe_2O_4$ is implicit. The reaction can therefore be stated as

$$NiFe_2O_4 + ZnO + Fe_2O_3 \rightarrow 2Ni_{0.5}Zn_{0.5}Fe_2O_4,$$

as opposed to a $NiFe_2O_4 + ZnFe_2O_4$ process. ii) The X-ray diffraction peaks shifted to lower 2θ angle as the heat treatment temperature increased from 400 to 500°C (Fig. 7). In the case of the precursor heat treated at 400°C, the lattice constant of $Ni_{0.5}Zn_{0.5}Fe_2O_4$ is almost identical to that of pure $NiFe_2O_4$. The increase in the lattice constant as a function of the heat treatment temperature suggests that more Zn^{2+} is incorporated into $NiFe_2O_4$ as temperature is increased. This further suggests that $Ni_{0.5}Zn_{0.5}Fe_2O_4$ forms as the result of a simultaneous reaction between $NiFe_2O_4$, ZnO and Fe_2O_3. Since the decomposition tem-

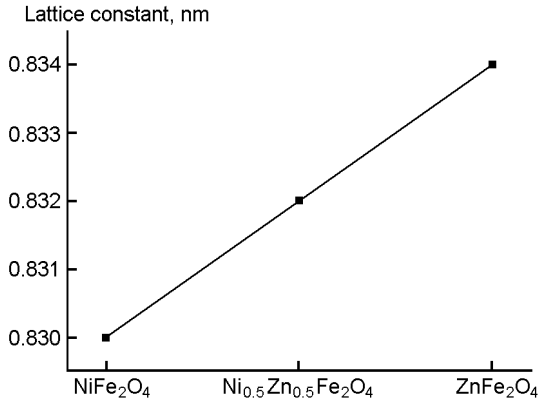

Fig. 7. Lattice constant of Ni–Zn ferrite measured from the XRD patterns of Ni–Zn ferrite precursors heat treated at 500°C with a isothermal heating for 2 h.

perature of the iron citric acid complex is low, nanocrystalline Fe_2O_3 and Zn coexist in the temperature range 400–500°C. In this case, a reaction between them is difficult before a complete decomposition of the hydrozincite is achieved at high temperature. The hydrozincite, which has not yet decomposed to an oxide, appears to hinder the reaction with Fe_2O_3. From this point of view, the solid state reaction between nanocrystalline oxides of ZnO and Fe_2O_3 might be easier than the reaction between iron and zinc citric acid complexes.

Fig. 8 shows the TEM observation of $NiFe_2O_4$ (Ni ferrite), $ZnFe_2O_4$ (Zn ferrite) and $Ni_{0.5}Zn_{0.5}Fe_2O_4$ (Ni–Zn ferrite) after a heat treatment of the precursors at 500°C for 2 h. As shown in the photographs, the particles are about 25 nm in diameter with spherical morphologies.

Particle size dependent magnetic characteristics. Fig. 9 shows the TEM micrographs of nanocrystalline $Ni_{1-x}Zn_xFe_2O_4$ ($0.0 \le x \le 1.0$) powders. Powders with average particle sizes of about 7 nm were obtained by the coprecipitation method. In order to obtain coarse nanocrystalline powders (around 100 nm), the powder prepared by the citrate precursor method was heat treated at 800°C for 2 h. Powders prepared by the citric precursor method with the particle sizes around 25 nm (Fig. 8) were also employed. The particle size was not dependent on the composition of $Ni_{1-x}Zn_xFe_2O_4$ when the powder preparation method was identical, and all of the powders exhibited nearly spherical morphologies.

Fig. 10 shows the X-ray diffraction patterns of the calcined $Ni_{1-x}Zn_xFe_2O_4$ powders prepared by various methods. Broad peaks at positions corresponding to the Ni–Zn ferrite were observed when the mean particle size is around 7 nm as shown in Fig. 10(a). When the mean particle sizes of Ni–Zn ferrites are increased from 7 to 25 and 100 nm, the width of the main diffraction peaks of Ni–Zn ferrite narrowed. The particle size, calculated from X-ray peak broadening using the Scherrer equation [17] agreed well with the values estimated from the TEM observation. The main diffraction peaks of Ni–Zn ferrite shifted to lower 2θ angles as the amount of Zn was increased, indicating an increase in the lattice constant due to the larger ionic radius of Zn^{2+} (0.74 Å) relative to that of Ni^{2+} (0.69 Å). Fig. 11 shows the magnetization hysteresis loops of $NiFe_2O_4$, $Ni_{0.5}Zn_{0.5}Fe_2O_4$, and $ZnFe_2O_4$ with particle sizes around 7 nm, 25 nm and 100 nm measured at 15,000 Oe and 300 K. In the case of $NiFe_2O_4$ with a particle size around 7 nm, the saturation magnetization (M_s) was found to be around 11.05 emu/g which was lower than that of the $NiFe_2O_4$ powders of 100 nm (48.44 emu/g). The decrease in the M_s of Ni ferrite with decreasing particle size has been previously reported [18–20]. In the

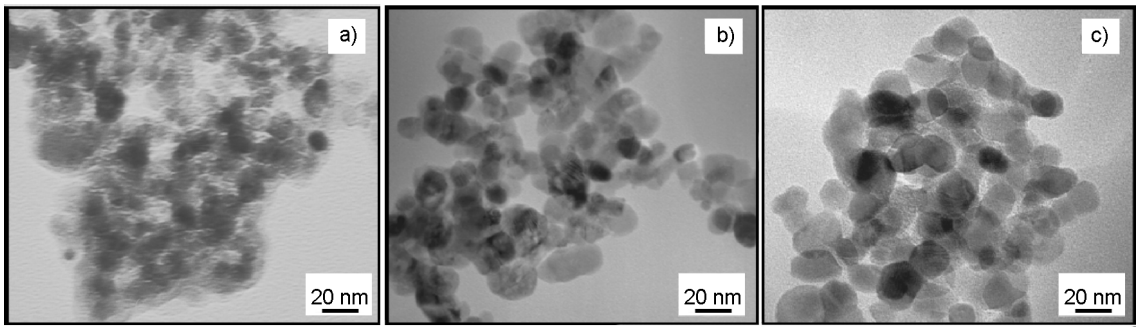

Fig. 8. TEM photographs of $NiFe_2O_4$, $ZnFe_2O_4$ and $Ni_{0.5}Zn_{0.5}Fe_2O_4$ after a heat treatment of the precursors at 500°C for 2 h; (a) $NiFe_2O_4$, (b) $ZnFe_2O_4$, and (c) $Ni_{0.5}Zn_{0.5}Fe_2O_4$.

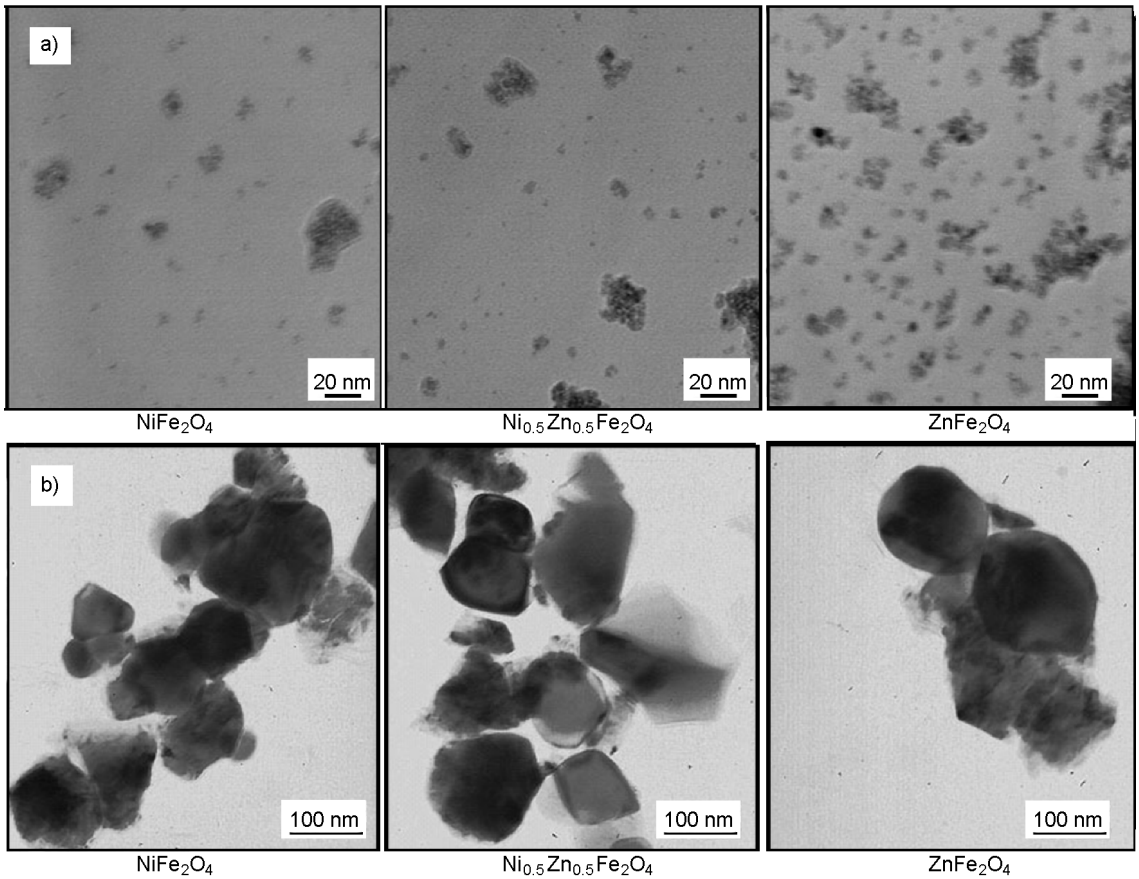

Fig. 9. TEM micrographs of nanocrystalline $Ni_{1-x}Zn_xFe_2O_4$ ($0.0 \le x \le 1.0$) powders with particle sizes of approximately (a) 7 nm and (b) 100 nm, (a) and (b) were calcined at 300 and 800°C for 2 h, respectively.

case of $Ni_{0.5}Zn_{0.5}Fe_2O_4$, the trend of the M_s was very similar to that of $NiFe_2O_4$. On the other hand, in the case of $ZnFe_2O_4$ with a particle size around 7 nm, M_s was around 9.66 emu/g which was higher than that of the $ZnFe_2O_4$ powders of 100 nm (2.40 emu/g).

Table summarizes the coercivity (H_c) values of nanocrystalline $Ni_{1-x}Zn_xFe_2O_4$ ($0.0 \le x \le 1.0$) with particle sizes around 7 nm, 25 nm and 100 nm. The coercivity of the ferrite powders exhibited a strong dependence on particle size. As shown in Table, the overall coercivity of nanocrystalline $Ni_{1-x}Zn_xFe_2O_4$ ($0.0 \le x \le 1.0$) decreased with decreasing particle size. However, the coercivity of 7 nm Ni–Zn ferrites did not reach zero. As the particle size is reduced, coercivity typically increases, goes through a maximum, and then trends toward zero [3]. Below a critical diameter D_c, which is not well defined, the particles become single domains, and in this size range the coercivity reaches a maximum. On the other hand, as the particle size decreases below D_c, the coercivity decreases due to thermal effects, according to

$$H_c = g - \frac{h}{D^{3/2}},$$

where g and h are constants. Below a critical diameter D_p the coercivity is zero, again because of thermal effects, which are now

Table. Coercivity of nanocrystalline $Ni_{1-x}Zn_xFe_2O_4$ ($0.0 \le x \le 1.0$) as a function of particle size.

Composition	Coercivity (Oe)		
	7 nm	25 nm	100 nm
$NiFe_2O_4$	153.6	153.6	233
$Ni_{0.8}Zn_{0.2}Fe_2O_4$	138.8	140.4	189.2
$Ni_{0.6}Zn_{0.4}Fe_2O_4$	112	124.2	116
$Ni_{0.5}Zn_{0.5}Fe_2O_4$	99.75	121.4	128.7
$Ni_{0.4}Zn_{0.6}Fe_2O_4$	115.2	117.8	132.6
$Ni_{0.2}Zn_{0.8}Fe_2O_4$	108.3	117.5	113.6
$ZnFe_2O_4$	281.2	298.6	568.9

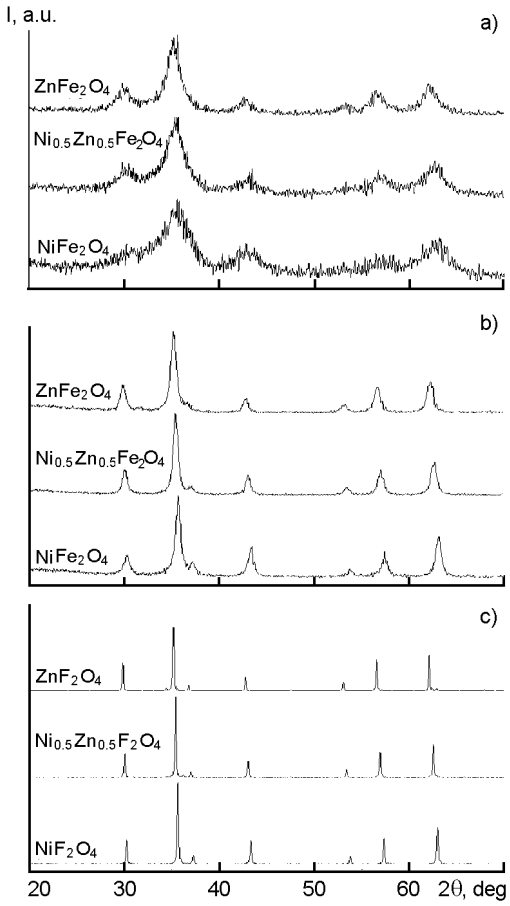

Fig. 10. XRD patterns of nanocrystalline $Ni_{1-x}Zn_xFe_2O_4$ ($0.0 \le x \le 1.0$) powders as functions of particle size and x.

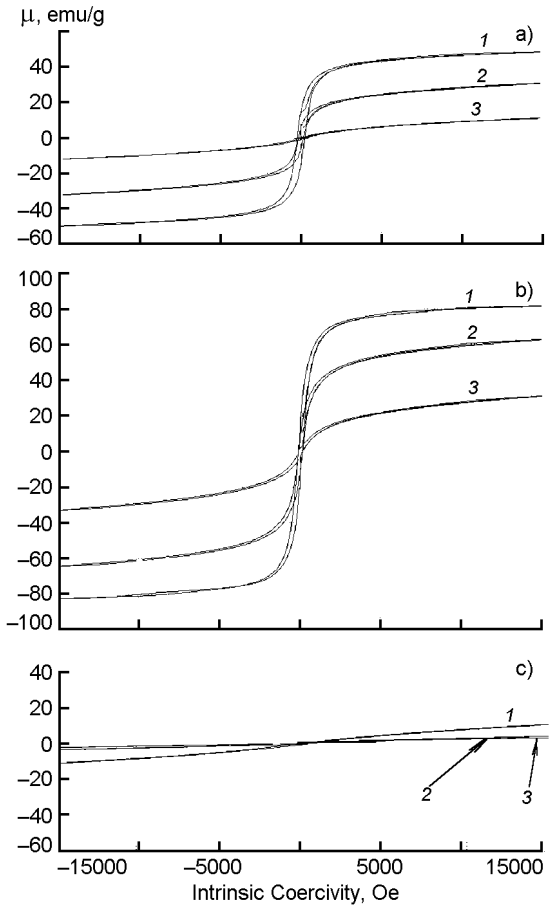

Fig. 11. Magnetization hysteresis loops of (a) $NiFe_2O_4$, (b) $Ni_{0.5}Zn_{0.5}Fe_2O_4$, and (c) $ZnFe_2O_4$ as a function of particle size: *1*– 7 nm; *2* – 25 nm; *3* – 100 nm.

strong enough to spontaneously demagnetize a previously saturated assembly of particles. Such particles are termed superparamagnetic [1]. From the coercivity values, the particle sizes of 7 nm and 25 nm are thought to be within the single domain region for the case of Ni–Zn ferrite because the coercivity increased as the particle size increased from 7 to 25 nm. Even though particle sizes of 7 and 25 nm are extremely small, superparamagnetic behavior was not observed since the coercivity of the Ni–Zn ferrite powders was not zero.

Fig. 12 shows the saturation magnetization of nanocrystalline $Ni_{1-x}Zn_xFe_2O_4$ ($0.0 \le x \le 1.0$) powders as a function of particle size. The saturation magnetization of nanocrystalline Ni–Zn ferrites with particle sizes around 25 nm and 100 nm remained almost the same with that of bulk ferrite [2]. In the case of $NiFe_2O_4$ and $Ni_{0.5}Zn_{0.5}Fe_2O_4$ the magnetization greatly decreased as the particle size decreased. In the case of 25 nm and 100 nm $ZnFe_2O_4$, the magnetization was almost zero as expected and reported earlier [2]. However, in the case of 7 nm $ZnFe_2O_4$, the saturation magnetization was not zero and revealed a higher value than that of the coarser $ZnFe_2O_4$ particles.

At this point, we should consider the fraction of atoms exposed at the surface from a theoretical viewpoint because the surface area of powders is a function of particle size, and the randomness and/or disorder of cations near the surface of nanocrystalline powders will exhibit a strong particle size dependence. Fig. 13 shows calculated surface:bulk ratios as a function of particle size under the assumptions that the ions are hard spheres with a radius of 0.1 nm and the crystal assumes a faced-centered cubic (FCC) structure; FCC is close-packed structure with an atomic pack-

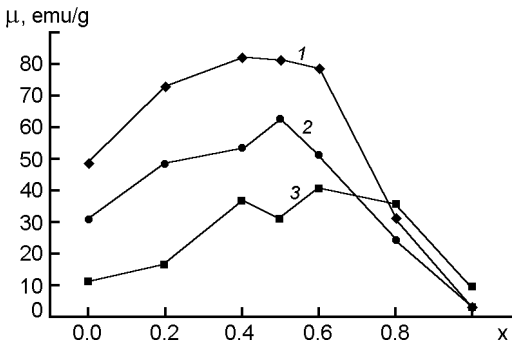

Fig. 12. Saturation magnetization of nanocrystalline $Ni_{1-x}Zn_xFe_2O_4$ ($0.0 \le x \le 1.0$) powders as a function of particle size: *1*– 100 nm; *2* – 25 nm; *3* – 7 nm.

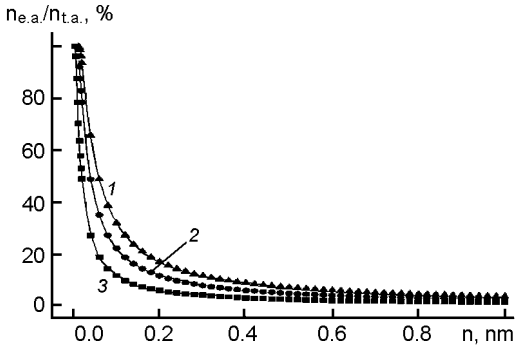

Fig. 13. Calculated surface to bulk ratios as a function of particle size in Ni–Zn ferrite: *1* – three layers exposed to surface, *2* – two layers exposed to surface and *3*— one layer exposed to surface.

ing factor of 0.74. According to the calculation, for a case when the outermost ions in a 7 nm particle are exposed, the surface to volume ratio is approximately 18 %, indicating that 18 % of all atoms in the crystallite are exposed at the surface. Assuming that the second and third layers are also considered as being located at the surface, the surface to volume ratio increase. In nanocrystalline solids a heterogeneously distributed disorder is generated by interrupting the periodicity of crystals by surfaces [21]. Because the broken bonds of atoms at the surface destabilize the crystal structure, ionic disordering may be occurring at the surface of ultrafine particles. From this point of view, the magnetic properties of in nano or atomic scale materials should differ from those of bulk or micrometer scale materials.

Disordering at the surfaces of spinels has been theoretically investigated [22]. Changes in magnetic properties due to cation disorder have been reported for mechanically activated Ni ferrite [23] and Zn ferrite quenched from high temperature [24] when compared to the micron-sized analogs. Therefore, the higher magnetization of 7 nm $ZnFe_2O_4$ powders relative to that of 25 and 100 nm, as observed in Figs. 11 and 12 is likely due to the cation-disordered structure resulting from random occupation and/or exchanges of Ni^{2+}, Zn^{2+} and Fe^{3+} ions between A and B-sites of the spinel structure.

In conclusion, in the synthesis of Ni–Zn ferrites by the citric precursor method, the different decomposition temperatures of nickel and zinc citric acid were found to affect the reaction kinetics, leading to the formation of Ni ferrite and Zn ferrite. Single-phase $NiFe_2O_4$ was produced directly when crystallization was initiated from an amorphous precursor. $ZnFe_2O_4$ was formed at 500°C from the reaction between Fe_2O_3 and ZnO phases that were first formed at 400°C. In those reactions involving Zn citric acid, organic substances bound to Zn^{2+} required significantly higher temperatures to achieve decomposition than the other metal citric acid complexes; reactions involving Zn citrate were consequently retarded. Concerning the particle size dependent magnetic characteristics, the saturation magnetization decreased as the particle size decreased in the case of $NiFe_2O_4$ and $Ni_{0.5}Zn_{0.5}Fe_2O_4$. However, in the case of $ZnFe_2O_4$, the saturation magnetization increased as the particle size decreased. Since ultrafine particles have considerable fraction of structurally unstable atoms exposed at their surface, the phenomenon seems to be the result of random occupation and/or exchanges of Ni^{2+}, Zn^{2+} and Fe^{3+} ions between A- and B-sites of the spinel structure.

Acknowledgement.

This work was supported by Korea Science and Engineering Foundation through the Research Center for Advanced Magnetic Materials at Chungnam National University. We also acknowledge funding from the Defense Advanced Research Projects Agency through Grant HR0011-05-1-0031.

References

1. B.D.Cullity, Introduction to Magnetic Materials, Addison Wesley, Reading, MA (1972).
2. W.D.Kingery, H.K.Bowen, D.R.Uhlmann, Introduction to Ceramics, John Wiley & Sons, New York (1960).
3. T.Tsutaoka, M.Ueshima, T.Tokunaga, T.Nakamura, *J. Appl. Phys.*, **78**, 3983 (1995).

4. K.J.Klabunde, J.Stark, O.Koper et al., *J. Phys. Chem.*, **100**, 12142 (1996).
5. St.Fischer, C.Michalk, W.Topelmann, H.Scheler, *Ceram. Intern.*, **18**, 317 (1992).
6. M.P.Morales, S.Veintemillas-Verdaguer, M.I.Montero, C.J.Serna, *Chem. Mater.*, **11**, 3058 (1999).
7. T.Hyeon, S.S.Lee, J.Park, *J. Am. Chem. Soc.*, **123**, 12798 (2001).
8. X.Huang, Z.Chen, *J. Magn. Magn. Mater.*, **280**, 37 (2004).
9. H.W.Wang, S.C.Kung, *J. Magn. Magn. Mater.*, **270**, 230 (2004).
10. C.Upadhyay, D.Mishra, H.C.Verma et al., *J. Magn. Magn. Mater.*, **260**, 188 (2003).
11. E.E.Sileo, R.Rotelo, S.E.Jacobo, *Physica B., Conden. Matter.*, **320**, 257 (2002).
12. Y.Hayashi, T.Kimura, T.Yamaguchi, *J. Am. Ceram. Soc.*, **69**, 322 (1986).
13. S.B.Cho, K.I.Kwon, K.K.Choi et al., *J. Am. Ceram. Soc.*, **29**, 177 (1992).
14. JCPDS: Joint Committee on Powder Diffraction Standards, Powder Diffraction File, International Center for Diffraction Data, Swarthmore, PA, card 39-1346.
15. JCPDS: Joint Committee on Powder Diffraction Standards, Powder Diffraction File, International Center for Diffraction Data, Swarthmore, PA, card 33-0664.
16. J.S.Kim, I.B.Kim, H.C.K and Y.K.Hong, *J. Am. Ceram. Soc.*, **29**, 942 (1992).
17. B.D.Cullity, Elements of X-ray Diffraction, Addison-Wesley, Reading, MA (1978).
18. A.H.Morrish, K.Haneda, *J. Appl. Phys.*, **52**, 2496 (1981).
19. K.Haneda, A.H.Morrish, *J. Appl. Phys.*, **63**, 4258 (1988).
20. Y.Kinemuchi, K.Ishizaka, H.Suematsu et al., *Thin Solid Films*, **407**, 109 (2002).
21. H.Gleiter, *Adv. Mater.*, **4**, 474 (1992).
22. S.C.Parker, D.J.Harris, F.M.Higgins et al., Atomic Simulation of Surfaces and Interfaces in Ionic Solids, in: Ceramic Interfaces edited by R.Smart and J.Nowotney, IOM Communications (1998), p.45.
23. Z.H.Zhou, J.M.Xue, J.Wang et al., *J. Appl. Phys.*, **91**, 6015 (2002).
24. K.Tanaka, M.Makita, Y.Shimizugawa et al., *J. Phys. Chem. Solids*, **59**, 1611 (1998).

Хімічний синтез нанокристалічних Ni-Zn феритів та їхні магнітні характеристики

Чжонг-Чул Лі, Д. Карунту, Чжун-Юнь Лі, Чжеонг-Чжу Кім, Б. Кашинг, В.Голуб, Санг-Хі Чо, Ч.О'Коннор

Методом цитратів-прекурсорів синтезовано нанокристалічні порошки $Ni_{1-x}Zn_xFe_2O_4$ та розглянуто послідовність реакцій у цьому процесі. Дослідження послідовності реакцій показало, що безпосередньо після термічного розкладу цитратів металів утворювалася фаза $NiFe_2O_4$. Однак у випадку $ZnFe_2O_4$ при розкладі цитратів металів при низькій температурі спочатку утворювалися ZnO та Fe_2O_3. Потім у процесі термообробки при 500°C протягом 2 год одержано єдину фазу $ZnFe_2O_4$. З іншого боку, з метою дослідження впливу розміру частинок на характеристики Ni-Zn феритів нанокристалічні порошки $Ni_{1-x}Zn_xFe_2O_4$ з розмірами частинок приблизно 7, 25 та 100 нм було одержано співосадженням та методом цитратів-прекурсорів. Виявлено істотні відмінності у магнітних характеристиках ультратонких (7 нм) та грубозернистих (100 нм) нанокристалічних феритів. Ці відмінності приписано катіонному розупорядкуванню на поверхнях частинок, переважна роль якого зростає при зменшенні розмірів частинок.